Preprints of the 19th World Congress
The International Federation of Automatic Control
Cape Town, South Africa. August 24-29, 2014

Optical-Flow Based Strategies for Landing VTOL UAVs in Cluttered Environments

Lorenzo Rosa * **Tarek Hamel** ** **Robert Mahony** ***
Claude Samson ****

* *L. Rosa is with the Dipartimento di Ingegneria Informatica, Automatica e Gestionale, Sapienza University of Rome, Italy.* rosa@diag.uniroma1.it
** *T. Hamel is with I3S UNS CNRS Lab* thamel@i3s.unice.fr
*** *R. Mahony is with the Research school of Engineering, Australian National University, Australia.* Robert.Mahony@anu.edu.au
**** *C. Samson is with INRIA Sophia/I3S UNS CNRS* claude.samson@inria.fr , csamson@i3s.unice.fr

Abstract: This paper considers the question of landing an Unmanned Aerial Vehicles (UAV) using a single monocular camera as the primary exteroceptive sensing modality. The proposed control law is based on tracking a single point feature, representing the desired landing point on a ground plane, along with optical flow computed over the full image. The bearing of the desired landing point is used as a driving term to force convergence, while the optical flow is used to provide a damping force that guarantees both obstacle avoidance as well as damping the convergence of the vehicle to the ground plane ensuring a soft touchdown. A detailed analysis of the system closed-loop dynamics is undertaken and the response of the system is verified in simulation.

Keywords: Aerial Robotics, UAV, VTOL, visual servo control, optical flow, landing.

1. INTRODUCTION

Autonomous aerial vehicles (UAVs) are a transformative technology in modern society, providing unparalleled capability to undertake difficult, dangerous and dull surveillance and monitoring tasks crucial to maintenance of infrastructure, agricultural operations and disaster recovery, to name just a handful of application domains. To perform a fully autonomous flight, an UAV requires the ability to take-off, navigate to, and accomplish a given task, and finally return to base and land. Many tasks require the vehicle to land, or at least approach and touch, its destination, and complex or long-lasting missions might require intermediate landing and taking-off operations (e.g. battery/fuel refill). Such manoeuvres generally need to be undertaken in unsurveyed, cluttered environments, and often where GPS signals are unreliable or unavailable. This is especially the case for Vertical Take-Off and Landing (VTOL) vehicles, such as helicopters and multi-rotor systems, that are likely to be used in tandem with ground based vehicles and other technologies, as in Michael et al. (2012), in extended disaster recovery or other types of missions. Classical landing control strategies require estimation of the full state of the vehicle, along with a model of the landing environment (see for example Flores and Milam (2006); Geyer and Johnson (2006); Meister et al. (2009); Andert et al. (2011)). If only a camera is available for state estimation then the vehicle pose must be estimated by using visual data (Lee et al., 2012; Davison et al., 2011; Kaiser et al., 2010; Courbon et al., 2010; Milford et al., 2011; Blösch et al., 2010). An alternative approach is to use the natural properties of optical flow to provide a strong visual cue for obstacle avoidance and landing regulation (Srinivasan et al., 2000; Koenderink and van Doorn, 1987; Hérissé et al., 2008; Chahl et al., 2004; Srinivasan et al., 2000; Ruffier and Franceschini, 2004). Optical flow is also a powerful cue for terrain following (Humbert et al., 2005; Ruffier and Franceschini, 2005) and obstacle avoidance (Geyer and Johnson, 2006; Green and Oh, 2008; Beyeler et al., 2009). A good review of prior work in robotics applications that exploit optical flow is given by McCarthy et al. (2012). A key advantage of control strategies that are based on optical flow is that they also deal well with dynamic environments such as a moving landing surface (Hérissé et al., 2010, 2012) in contrast to approaches that require modeling of the environmental motion (Marconi et al., 2002). A disadvantage of control algorithms based on optical flow and visual data in general is the complexity of providing rigourous stability analysis of the closed loop system, especially in the case where the system has non-trivial dynamics, as is the case with flying vehicles.

In this paper, we propose a landing control algorithm for a VTOL UAV based on visual data obtained from a monocular camera coupled with the usual suite of sensors present in a standard Inertial Measurement Unit (IMU) that is common on all modern UAVs. We provide a detailed analysis of the closed-loop response of the system and prove asymptotic stability of the pose to the desired

landing point, corresponding to a smooth touch down. We first consider the case where there are no obstacles and propose a reformulation of the controller formerly developed by Hérissé et al. (2010, 2012) to include a target landing point. The proposed control consists of a driving term that acts as a constant force driving the vehicle in the direction of the observed target point, based on the bearing measurement of the target, coupled with a damping proportional to optical flow measured over the whole ground plane. The natural tradeoff between velocity and distance inherent in optical flow ensures a stable soft touchdown of the closed-loop system. We then consider obstacles present in the flying space by including additional damping terms associated with divergence of the optical flow derived from the obstacle. To simplify the mathematical formulation of the problem, the ground plane is assumed to be flat and obstacles are modeled as spheres in space. The goal of this paper is to provide a detailed theoretic analysis of the system response rather than tackle some of the practical issues of implementation. To this end the visual target observation and optical flow measurements are abstracted and written in terms of the vehicle state for the purposes of the analysis. Simulations of the closed-loop dynamics are provided to demonstrate the performance of the proposed algorithm.

The content is organized as follows: Section 2 describes the landing task; the differential equations representing the motion model for small-scale VTOLs and the modelling of the environment. Section 3 proposes a control law for the landing task in obstacle-free environments and provides a detailed stability analysis. Section 4 considers the case where there are obstacles in space and provides an analysis for the proposed control. Section 5 reports on some simulation results for both obstacle-free and cluttered environments. The paper concludes with some final comments in Section 6.

2. SYSTEM AND ENVIRONMENT MODELLING

In this section we introduce the model used throughout the document to describe the vehicle dynamics and the environment.

Consider a Vertical-Take-Off-and-Landing (VTOL) UAV vehicle equipped with an Inertial Measurement Unit (IMU) and suitable filtering algorithms to provide reliable estimates of attitude and rotational velocities, as well as a camera, an exteroceptive passive sensor whose output is rich in information. We assume that the vehicle is equipped with vision processing capability to identify a point-feature target and compute optical flow over the full image (Horn and Schunck, 1981).

A complete model of a VTOL aircraft includes gyroscopic and aerodynamics effects, as well as aerodynamic disturbances. In order to simplify the analysis, we neglect all second order terms (Mahony and Hamel, 2004). The neglected aerodynamics forces are dissipative and do not significantly effect the closed-loop response. Rotational dynamics of small-size VTOL vehicles are usually faster than translational ones, leading to a hierarchical control design methodology. The natural time-scale separation between the translational dynamics (slow time-scale) and the orientation dynamics (fast time-scale) allows one to design decoupled position and orientation controllers (Khalil, 2002; Hérissé et al., 2012). The high-gain attitude control effectively dominates the attitude dynamics of the vehicle and allows one to consider a pure translational model

$$\begin{aligned} \dot{\xi} &= v \\ m\dot{v} &= mge_3 - TRe_3\,, \end{aligned} \tag{1}$$

in which ξ and v represent the UAV position and velocity respectively, both expressed in an inertial frame with the third direction aligned with the gravitational field, m represents the mass of the VTOL-UAV (supposed constant), g is the magnitude of the gravity force acting on the vehicle and e_3 is the third canonical basis vector. The variable T represents the thrust magnitude and R is the rotation matrix representing the orientation of the body-fixed frame with respect to the inertial frame. The high-gain attitude control assumption means that the rotation R can be viewed as a control input and we write $u = -TRe_3$ to represent the resulting control input to the translational dynamics of the system

$$\begin{aligned} \dot{\xi} &= v \\ m\dot{v} &= mge_3 + u\,. \end{aligned} \tag{2}$$

In order to develop the dynamics equation of image points, in the following we suppose that the frame representing the position and orientation of the camera in the world frame is rigidly attached to the body-fixed frame, such that the linear transformation relating them degenerates to the identity matrix and their dynamics are the same. Projections of world points on the image surface are points, usually called *point features* or *features*, whose dynamics depend on the geometry of the image surface and on the physical parameters of the camera. A common choice in the aerial robotics field is to model the dynamics of the point features by using the *spherical projection* model for a *calibrated* camera as shown by Ma et al. (2004). Consider a reference frame attached to the camera. If $\bar{P}$ is a generic point in the 3-D space, we denote with P the vector connecting the centre of the camera reference frame to the point $\bar{P}$ and with p the unit vector representing the direction of P, i.e. its projection on a sphere of unit radius, that represents the spherical image surface. The expression of the vector p and its derivative are

$$p = \frac{P}{|P|}\,, \quad \dot{p} = -\frac{\pi_p}{|P|}v, \tag{3}$$

where [1]

$$\pi_p = (I_3 - pp^\top) \tag{4}$$

is the projector in the space tangent to the spherical image surface at point p, having the following properties

$$p^\top \pi_p = \pi_p\, p = 0 \quad \text{and} \quad \pi_p^2 = \pi_p \tag{5}$$

We will assume that the desired landing point $\bar{P}_L$ is contained locally in a planar surface whose normal η is known or can be estimated from image features (see, for instance, Ma et al. (2004)). In general, the normal direction cannot be easily determined unless a good knowledge of the environment is available. There are, however, certain special cases where it is relatively straightforward to extract it, such as the situation where the target lies on a flat ground. In this case η is obviously the gravitational direction e_3 and can be directly provided by the IMU sensor.

[1] The symbol I_3 represents the identity matrix of dimension 3 by 3.

A soft landing manoeuvre consists in progressively reducing the distance between the vehicle and the desired landing point, ensuring it reaches the zero value with zero speed. The environment enforces a physical constraint on the vehicle height: it has to be all time strictly positive. Indeed, the desired landing point will always lie on the boundary of the admissible region of the space, an asseveration that requires careful consideration in the stability analysis.

We approximate the cluttered environment by a collection of fixed spherical objects. For a given obstacle, let $\bar{P}_o$ denote the closest point on the surface of the obstacle to the camera. Let P_o be the vector from camera to $\bar{P}_o$ and define $d_o = |P_o|$ to be the distance from camera to the obstacle. The vector p_o denotes the projection of P_o onto the spherical image surface, $p_o = P_o/d_o$. Note that p_o is orthogonal to the tangent plane of the spherical obstacle. We assume that the de-rotated optical flow Φ is computed at all points in the image. The divergence of the optical flow is a scalar field that can be computed from the optical field using either differentials of the flow or a vector convolution. Locally around p_o in the image the divergence of the optical flow is related to the scaled rate of change of distance (Coombs et al., 1998)

$$\mathrm{div}\Phi(p_o) = -2\frac{\dot{d}_o}{d_o}. \tag{6}$$

In the sequel we will use the term $\dot{d}_o/d_o$ directly in the control rather than the flow divergence. In the same manner, denoting the flow over the projection of the ground plane spherical image by $\mathcal{D} \subset S^2$ one can show that

$$\frac{v}{h} = \Lambda \int_{\mathcal{D}} \Phi(p) dp$$

for a matrix $\Lambda > 0$ that can be computed from knowledge of the size of $\mathcal{D}$ (Hérissé et al., 2012) and where h is the distance from the camera to the landing surface plane in the normal direction η. We will again use the expression v/h in the control analysis rather than writing the dependence on the optical flow field directly. A key aspect of the optical flow measurements is that the resulting measurements always depend inversely on distance to the observed object as well as depending linearly on the camera velocity. This singularity in the velocity leads to much of the nice properties of optical flow as a cue for obstacle avoidance, but also causes significant complications in the analysis.

We will also use an integral over time of the flow divergence in the sequel

$$\begin{aligned}\bar{\gamma}_o(t) :&= -\frac{1}{2}\int_0^t \mathrm{div}\Phi(p_o)\, d\tau \\ &= \int_0^t \frac{\dot{d}_o(\tau)}{d_o(\tau)} d\tau = \ln\left(\frac{d_o(t)}{d_o(0)}\right)\end{aligned} \tag{7}$$

This quantity provides a rough measurement of the actual distance to the object that will be exploited for obstacle avoidance. To this aim, we will use

$$\gamma_o = \begin{cases} \bar{\gamma}_o & \bar{\gamma}_o < 0 \\ 0 & \text{otherwise} \end{cases}, \tag{8}$$

and produce a repulsive force only when $d_o(t) < d_o(0)$. We will assume further that an obstacle-free path to the landing point exists and that the landing point is visible at all times. Clearly this assumption will fail in highly cluttered environments, and hybrid control laws involving either a switching mechanism between different target points or the addition of feedforward driving terms can be considered to overcome this difficulty. This issue is beyond the scope of the present paper which focuses on the core nonlinear aspects of the problem. Real obstacles are not spherical either, and practical implementation of the proposed control laws will have to incorporate complementary mechanisms that minimize the effects of this approximation.

3. LANDING IN OBSTACLE-FREE ENVIRONMENTS

In this section, we consider the task of landing on a specified target in an obstacle-free environment. The proposed solution is a variant of the controllers formerly developed by Hérissé et al. (2010, 2012), which are proportional-integral nonlinear controllers based on optical flow data only. Using the fact that the landing point is specified, we avoid using the time-integration of the optical flow measurements in the control law (for stability purposes) by substituting this integral with the bearing $\xi/|\xi|$ to the landing point. Avoiding numerical integration is particularly useful in real applications for which optical flow measurement noise is not negligible, e.g. when the limited field of view does not allow for proper averaging of the measurements and yields the divergence of the integral.

Note that, given any desired landing point, one can use a simple change of coordinates and rewrite the system as if the landing point was the origin of the 3-D space. We will accordingly assume from now on that the desired landing point is $\bar{P}_L = (0,0,0)^\top$, which allow us to directly write the bearing as $\xi/|\xi|$.

Theorem 1. Consider the system (2) subjected to the control input

$$u_{\mathrm{L}} = -mge_3 - mk\left(\frac{v}{h} + \frac{\xi}{|\xi|}\right) \tag{9}$$

then, for any initial condition such that $h(0) > 0$ and for some $k > 0$ the following assertions hold

(1) $h(t) > 0\,, \forall t$ (implying that the dynamics of the closed-loop system are well defined $\forall t$);
(2) $h(t)$ and $\dot{h}(t)$ converge to zero asymptotically;
(3) $v(t)$ converges to zero asymptotically;
(4) $\xi(t)$ converges to zero asymptotically;
(5) the control law (9) is bounded $\forall t$.

The proof of the theorem is given in Appendix A.II.

It is worth noticing that, if we assume that the normal direction to the plane is known, the proposed control input can be computed by using IMU data, Optical Flow measurement and the image of the desired landing point.

4. LANDING AMONG OBSTACLES

Navigation and control of vehicles in cluttered environments is a central topic in the area of field robotics. Several solutions have been developed in the literature to cope with this problem. The most familiar approach is arguably the so-called *artificial potential fields* from Khatib (1986) where the key idea consists in building artificial repulsive

force fields that depend linearly on the inverse of the distance to the sensed obstacles. A key disadvantage of this approach is the possible presence of local minima that prevent the robot from reaching the goal (Adeli et al., 2011) and the need to build an accurate local map of the environment from sensor data (Borenstein and Koren, 1989). The latter point is particularly challenging in the case of an aerial robotic vehicle equipped with a sensor suite comprising only an inertial measurement unit and a camera.

An alternative solution is to exploit optical flow as a vision cue for obstacle avoidance (Nelson and Alloimonos, 1989; Ancona and Poggio, 1993; Coombs et al., 1998). The approach taken in this paper is to modify the control strategy presented in Section 3 by adding a term that is associated with divergent optical flow to ensure obstacle avoidance.

Consider a collection of n spherical objects as discussed in Section 2. Let $\bar{P}_i$ denote the closest point on the surface of the obstacle to the camera, $d_i = |P_i|$ and $p_i = P_i/d_i$. Recall the control input u_L of relation (9) that was proposed for the landing problem free of obstacles, and consider the following modified control

$$u = u_L + u_D, \qquad \text{with } u_D = \sum_{i=1}^{n} k_D \frac{\dot{d}_i}{d_i} p_i \tag{10}$$

where the term $(\dot{d}_i/d_i)p_i$ can be calculated in practice based from the measurement of the divergence of the optical flow (6). The time-derivative $\dot{d}_i = -v^\top p_i$ of the distance d_i to the obstacle is the projection of the vehicle's velocity vector along the direction p_i, and it is negative as the vehicle approaches the obstacle. Consider the standard storage function (also exploited in the proof of Th. 1, see eq. (A.8)),

$$\mathcal{L} = k|\xi| + \frac{|v|^2}{2},$$

whose time-derivative along any solution to the closed-loop system is

$$\dot{\mathcal{L}} = -k\frac{|v|^2}{h} - k_D \sum_{i=1}^{n} \frac{(p_i^\top v)^2}{d_i} \leq 0,$$

and which points out the fact that u_D is a dissipative term. Although contact with an obstacle cannot be ruled out, the rate of dissipation being inversely proportional to the distance to the obstacle, it is reasonable to expect that there will be no collision, i.e. that contact will occur with zero velocity. Now, it is also desirable that the dissipation induced by the divergence of optical flow does not trap the robot near an obstacle and prevents it from moving around the obstacle and from converging to the target. To this aim we propose a slight modification of the previous control law which consists in working out a small repulsive field around each obstacle. Let us introduce the following local potential function associated with the object with index i

$$\phi_i(d_i) = \begin{cases} k_R(d_i(t)\,(\gamma_i(t) - 1) + d_i(0)), & d_i < d_i(0) \\ 0, & d_i \geq d_i(0) \end{cases} \tag{11}$$

where k_R is a small positive gain ($k_R \ll k$), and γ_i is given by (8). Note that $\frac{d\phi_i(d_i)}{dd_i} = k_R\gamma_i$, then the repulsive force associated with this potential is given by

$$F_i(d_i) = k_R\gamma_i p_i\,. \tag{12}$$

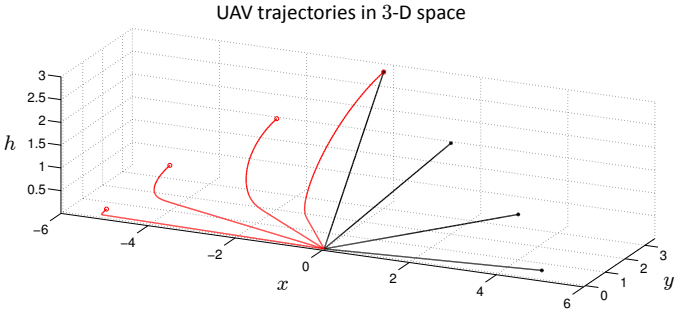

Fig. 1. Trajectories in the 3-D space (x-y-h), obstacle-free environment. Initial conditions: $v_1(0) = (0,0,0)^\top$, drawn in black, or $v_2(0) = (-1,0,-1)^\top$, drawn in red.

Since γ_i is negative near the obstacle, this force, even if it is small, tends to drive the vehicle away from the obstacle. For n visible obstacles in the environment, an obstacle-avoidance control input is obtained by summing up all repulsive forces

$$u_R = k_R \sum_{i=1}^{n} \gamma_i\, p_i. \tag{13}$$

Although undesired equilibria near the obstacles exist, we prove that these equilibria are unstable. More precisely, we show the following result.

Theorem 2. Consider the system (2) to which the control input

$$u = u_L + u_D + u_R. \tag{14}$$

is applied. Assume that the environment is populated by n ($n \geq 1$) spherical obstacles and assume also that there is no contact between the obstacles and the landing plane. Then, for any initial conditions such that $h(0) > 0$, there exists a small gain k_R such that the following assertions hold true

(1) $h(t) > 0\,, \forall t$ (implying that the dynamics of the closed-loop system are well defined $\forall t$).
(2) The set of equilibria

$$E_u = \left\{ (\xi^*, 0) \;\; s.t. \;\; k\frac{\xi^*}{|\xi^*|} = k_R \sum_{i=1}^{n} p_i(\xi^*)\gamma_i(\xi^*) \right\};$$

associated with the obstacles is unstable.

The proof is given in Appendix A.III.

5. SIMULATION RESULTS

In this section we show simulation results that illustrate the performance of the landing controller (9) and of its extension in the cluttered environment case (13). The measurements of the optical flow and of the bearing direction to the obstacles are intentionally corrupted by an additive Gaussian noise to show the robustness of the control scheme. We report two sets of simulation results: for an obstacle-free environment and for a cluttered one.

The first set of simulations concerns the application of control law (9) when the vehicle navigates in an obstacle free environment. Two different initial velocities, $v_1(0) = (0,0,0)^\top$ and $v_2(0) = (-1,0,1)^\top$, associated with different initial positions that span the (x,h)-plane are chosen. Initial conditions with zero velocity $v_1(0)$ yield straight line trajectories, drawn in black in Fig. 1. When

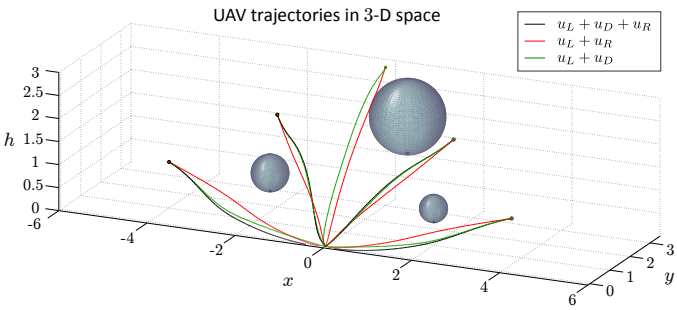

Fig. 2. Trajectories in the 3-D space (x-y-h) for different initial conditions. Comparison in the use of obstacle avoidance control.

the vehicle starts with non-zero velocity $v_2(0)$ it is initially driven away and heads towards the ground. In a short transient it recovers the convergence towards the landing point (drawn in red in Fig. 1). The damping phenomena which prevents the vehicle from colliding with the ground is more accentuated when the vehicle starts at very low height, h. This is due to the dissipative term $\frac{v}{h}$ which is all the much stronger that h is small and $|v|$ is large. The control gain was $k = 1$.

The second set of simulations considers the landing in a cluttered environment case and is reported in Fig. 2. The addition of the repulsive field (13) or damping control (10) to the landing control (9) modifies all system's trajectories. To show the effect of each contribution, we distinguish three cases: i) $u_L + u_D$ (green lines), ii) $u_L + u_R$ (red lines), iii) $u_L + u_D + u_R$ (black lines). The control gains are $k = 1$ and $k_D = 1$, and $k_R = 0.1$, the latter is chosen according to the condition $k_R \ll k$ discussed in Appendix A.III. Green and black lines (generated respectively by $u_L + u_D$ and $u_L + u_D + u_R$) are often superimposed, revealing that most of the obstacle avoidance action in (14) is due to u_D.

6. CONCLUSIONS AND FUTURE WORKS

This paper addresses the problem of landing a VTOL-UAV in obstacle-free or cluttered environments. The proposed control law exploits measurements issued from a camera attached to the vehicle and from an IMU, a common sensory suite for an unmanned aerial vehicle. The simulation results show the effectiveness of the control law in all environments. Spherical objects, placed at a non-zero height from the ground, are considered. Addressing the case of non-spherical objects would involve estimating the normal to their surface and would be a useful extension towards a real-world implementation of the proposed control strategies. Some further work is also needed for the case of cluttered environments, to extend the results of Theorem 2 to all possible cases. Clearly, a sound evaluation of what is needed to test these strategies in various environmental conditions and to improve them so as make them fully operational in practical situations requires experimenting on real small-scale UAVs.

ACKNOWLEDGMENTS

This work was supported by ANR-ASTRID project SCAR (ANR-12-ASTR-003) "Sensory Control of Aerial Robots".

REFERENCES

Adeli, H., Tabrizi, M.H.N., Mazloomian, A., Hajipour, E., and Jahed, M. (2011). Path planning for mobile robots using iterative artificial potential field method. *International Journal of Computer Science (IJCSI)*, 8(2), 28–32.

Ancona, N. and Poggio, T. (1993). Optical flow from 1d correlation: Application to a simple time-to-crash detector. In *Proceedings of the International Conference on Computer Vision*, 209–214.

Andert, F., Adolf, F., Goormann, L., and Dittrich, J. (2011). Mapping and path planning in complex environments: An obstacle avoidance approach for an unmanned helicopte. In *Proceeding of IEEE International Conference on Robotics and Automation*, 745–750.

Beyeler, A., Zufferey, J.C., and Floreano, D. (2009). Vision-based control of near-obstacle flight. *Journal of Autonomous Robots*, 201–219.

Blösch, M., Weiss, S., Scaramuzza, D., and Siegwart, R. (2010). Vision based mav navigation in unknown and unstructured environments. In *Proceedings of IEEE International Conference on Robotics and Automation*, 21–28.

Borenstein, J. and Koren, Y. (1989). Real-time obstacle avoidance for fast mobile robots. *IEEE Transactions on Systems, Man and Cybernetics*, 19(5), 1179–1187.

Chahl, J.S., Srinivasan, M.V., and Zhang, S.W. (2004). Landing strategies in honeybees and applications to uninhabited airborne vehicles. *International Journal of Robotics Research*, 101–110.

Coombs, D., Herman, M., Hong, T., and Nashman, M. (1998). Real-time obstacle avoidance using central flow divergence and peripheral flow. *IEEE Transactions on Robotics and Automation*, 14(1), 49–59.

Courbon, J., Mezouar, Y., Guenard, N., and Martinet, P. (2010). Vision-based navigation of unmanned aerial vehicles. *IEEE Transactions on aerospace and electronic systems*, 18, 789–7997.

Davison, A.J., Molton, I.D.R.N.D., and Stasse, O. (2011). Monoslam: Real-time single camera slam. *IEEE Transactions on pattern analysis and machine intelligence*, 29(6), 1052–1067.

Flores, M.E. and Milam, M.B. (2006). Trajectory generation for differentially flat systems via nurbs basis functions with obstacle avoidance. In *Proceeding of American Control Conference (ACC)*, 5769–5775.

Geyer, M.S. and Johnson, E.N. (2006). 3d obstacle avoidance in adversarial environments for unmanned aerial vehicles. In *AIAA Guidance, Navigation, and Control Conference and Exhibit*.

Green, W.E. and Oh, P.Y. (2008). Optic flow based collision avoidance. *IEEE Robotics & Automation Magazine*, 96–103.

Hérissé, B., Hamel, T., Mahony, R., and Russotto, F.X. (2010). The landing problem of a vtol unmanned aerial vehicle on a moving platform using optical flow. In *IEEE/RSJ International Conference on Intelligent Robots and Systems (IROS)*, 1600–1605.

Hérissé, B., Hamel, T., Mahony, R., and Russotto, F.X. (2012). Landing a vtol unmanned aerial vehicle on a moving platform using optical flow. *IEEE Transaction on robotics*, 28(1), 77–89.

Hérissé, B., Russotto, F.X., Hamel, T., and Mahony, R. (2008). Hovering flight and vertical landing control of a vtol unmanned aerial vehicle using optical flow. In *IEEE/RSJ International Conference on Intelligent Robots and Systems (IROS)*, 801–806.

Horn, B.K.P. and Schunck, B.G. (1981). Determining optical flow. *Artificial Intelligence*, 17, 185–203.

Humbert, J.S., Murray, R.M., and Dickinson, M.H. (2005). Pitch altitude control and terrain following based on bio-inspired visuomotor convergence. In *AIAA Conference on Guidance, Navigation and Control*.

Kaiser, M.K., Gans, N.R., , and Dixon, W.E. (2010). Vision-based estimation for guidance, navigation, and control of an aerial vehicle. *IEEE Transactions on aerospace and electronic systems*, 46(3), 1064–1077.

Khalil, H.K. (2002). *Nonlinear Systems*. Prentice-Hall.

Khatib, O. (1986). Real-time obstacle avoidance for manipulators and mobile robotics. *The International Journal of Robotics Research*, 5(1), 90–98.

Koenderink, J. and van Doorn, A. (1987). Facts on optic flow. *Journal of Biological Cybernetics*.

Lee, D., Ryan, T., and Kim, H.J. (2012). Autonomous landing of a vtol uav on a moving platform using image-based visual servoing. In *IEEE International Conference on Robotics and Automation*, 971–976.

Ma, Y., Soatto, S., Košeckà, J., and Sastry, S.S. (2004). *An Invitation to 3-D vision*. Springer.

Mahony, R. and Hamel, T. (2004). Robust trajectory tracking for a scale model autonomous helicopter. *International Journal of Robust and Nonlinear Control*, 14(12).

Marconi, L., Isidori, A., and Serrani, A. (2002). Autonomous vertical landing on an oscillating platform: an internal-model based approach. *Automatica*, 38, 21–32.

McCarthy, C., Barnes, N., and Mahony, R. (2012). A unified strategy for for landing and docking using spherical flow field divergence. *IEEE Transactions on Pattern Analysis and Machine Intelligence*, 34(5), 1024–1031.

Meister, O., Frietsch, N., Ascher, C., and Trommer, G.F. (2009). Adaptive path planning for vtol-uavs. *Aerospace and Electronic Systems Magazine, IEEE*, 24(7), 36–41.

Michael, N., Shen, S., Mohta, K., Mulgaonkar, Y., Kumar, V., Nagatani, K., Okada, Y., Kiribayashi, S., Otake, K., Yoshida, K., Ohno, K., Takeuchi, E., and Tadokoro, S. (2012). Collaborative mapping of an earthquake-damaged building via ground and aerial robots. *Journal of Biological Cybernetics*, 29, 832–841.

Milford, M.J., Schill, F., Corke, P., Mahony, R., and Wyeth, G. (2011). Aerial slam with a single camera using visual expectation. In *Proceedings of IEEE International Conference on Robotics and Automation*, 2506–2512.

Nelson, R.C. and Alloimonos, J.Y. (1989). Obstacle avoidance using flow field divergence. *IEEE Transactions on Pattern Analysis and Machine Intelligence*, 11(10), 11021106.

Ruffier, F. and Franceschini, N. (2004). Visually guided micro-aerial vehicle: automatic take off, terrain following, landing and wind reaction. In *Proceedings of IEEE International Conference on Robotics and Automation*.

Ruffier, F. and Franceschini, N. (2005). Optic flow regulation: the key to aircraft automatic guidance. *Journal of Robotics and Automation Systems*, 177–194.

Srinivasan, M., Zhang, S., Chahl, J.S., Barth, E., and Venkatesh, S. (2000). How honeybees make grazing landings on flat surfaces. *Journal of Biological Cybernetics*.

Appendix A

A.1 Preliminary technical lemmas

All time-dependent functions involved in the statements of these lemmas are assumed to be defined on $[0, +\infty)$ and continuous. The state variable x belongs to $\mathbb{R}^n$, with n a positive integer. Also, $o(t)$ denotes any bounded vector-valued function whose norm tends to zero when t tends to infinity.

Lemma 3. Consider the system

$$\dot{x} = -k(t)x + p(t)\,. \tag{A.1}$$

If $k(t)$ is positive $(\forall t)$ and tends to infinity, and if $|p(t)|$ is bounded, then (any solution) $x(t)$ (to this system) converges to zero.

Proof. The lemma's assessment is obvious after observing that, by replacing the time index t by the new time-scale index $s(t) := \int_0^t k(\tau)d\tau$ (note that s tends to infinity if and only if t also tends to infinity), the considered system rewrites as

$$\frac{d}{ds}x = -x + o(s)$$

with $o(s) := \frac{p(t)}{k(t)}$. This is a stable linear system perturbed by a vanishing additive perturbation.

Lemma 4. Consider the system

$$\dot{x} = -k(t)(\,(1 + o(t))\,x + p(t)\,)\,. \tag{A.2}$$

If $k(t)$ is positive $(\forall t)$ and tends to infinity, and if $|p(t)|$ is bounded, then $|x(t)|$ is bounded.

Proof. Again the proof of this lemma is quite simple after using the same change of time-scale index as for the previous lemma. This yields

$$\frac{d}{ds}x = -(1 + \bar{o}(s))x - \bar{p}(s)\,,$$

with $\bar{o}(s) = o(t)$ and $\bar{p}(s) = p(t)$. Since $(1 + \bar{o}(s))$ tends to 1, this is basically a stable linear system perturbed by a bounded additive perturbation.

Lemma 5. Consider the system

$$\dot{x} = -k(t)(\,(1 + o(t))\,x + p(t)\,)\,, \tag{A.3}$$

If $k(t)$ is positive $(\forall t)$ and tends to infinity, and if $|p(t)|$, $|\dot{p}(t)|$, and $k(t)o(t)$ are bounded. Then, $(x(t) + p(t))$ converges to zero as t goes to infinity.

Proof. Define $y := x + p$, then

$$\begin{aligned}\dot{y} &= -k(t)([1 + o(t)]x + p) + \dot{p}\\ &= -k(t)[1 + o(t)]y + k(t)o(t)p + \dot{p}\,.\end{aligned}$$

and a direct application of Lemma 3 yields the desired result.

Lemma 6. Consider two positive functions $\alpha(t)$ and $\beta(t)$ such that

$$\lim_{t\to\infty} \int_0^t \alpha(s)\,ds \;=\; +\infty\,, \qquad \lim_{t\to\infty} \beta(t) = 1\,,$$

then

$$\lim_{t\to\infty} \int_0^t \alpha(s)\beta(s)\,ds \;=\; +\infty.$$

Proof. There exists a time t^* such that $\beta(t) > \beta_0 > 0$, $\forall\, t > t^*$. Therefore, when $t > t^*$ one has

$$\int_0^t \alpha(s)\beta(s)\,ds > \int_0^{t^*} \alpha(s)\beta(s)\,ds \;+\; \beta_0 \int_{t^*}^t \alpha(s)\,ds\,,$$

with the last term in the right-hand side of the inequality converging, by assumption, to infinity.

A.II Proof of Theorem 1

Given the control (9) applied to the system (2), the equation of the closed-loop system is

$$\ddot{\xi} = -k\left(\frac{\dot{\xi}}{h} + \frac{\xi}{|\xi|}\right) = -k\left(\frac{\dot{\xi}}{h} + \alpha\frac{\xi}{h}\right), \qquad (A.4)$$

with

$$\alpha(t) = \frac{h(t)}{|\xi(t)|}, \qquad \alpha(t) \in (0,1],\ \forall t. \qquad (A.5)$$

Proof of item 1: The vehicle is initially above the target, i.e. $h(0) > 0$. Given an (any) initial condition $(\xi(0), v(0))$, as long as $h(t)$ does not reach zero, the solution to the above equation is well defined and unique. Let us first show that $h(t)$ cannot reach zero in finite time. By definition h is the third component of ξ. Therefore, in view of (A.4), the time-evolution of h is given by

$$\ddot{h} = -k\left(\frac{\dot{h}}{h} + \alpha\right). \qquad (A.6)$$

Integration of both sides of this equality yields

$$\dot{h}(t) = \dot{h}(0) - k\ln\left(\frac{h(t)}{h(0)}\right) - k\int_0^t \alpha(s)\,ds\,. \qquad (A.7)$$

This relation is valid as long as $h(t) \neq 0$. Now, consider the following positive storage function

$$\mathcal{L} = k\,|\xi| + \frac{|v|^2}{2}\,, \qquad (A.8)$$

whose time-derivative along a solution to System (A.4) is

$$\dot{\mathcal{L}} = -k\frac{|v|^2}{h} \leq 0\,. \qquad (A.9)$$

One deduces from the previous two relations that $|\xi|$ $(\geq h)$ and $|v|$ $(\geq |\dot{h}|)$ are uniformly bounded with respect to the initial condition, as long as the solution to the system is defined, i.e. as long as h remains positive. If we assume that h reaches zero at the finite time-instant $T_s > 0$, then the term $\ln\left(\frac{h(t)}{h(0)}\right)$ appearing in the equality (A.7) tends to infinity when t tends to T_s, whereas all other terms involved in this equality remain bounded. This assumption thus yields a contradiction. Therefore h is never equal to zero, and the solution to System (A.4) is well defined and unique for $t \in [0, \infty)$.

Proof of item 2: Using the following change of variables

$$z(t) = h(t)\,\mathtt{exp}\left(\frac{\dot{h}}{k}\right), \qquad (A.10)$$

one gets $\dot{z}(t) = -\alpha(t)\,z(t)$, a first order differential equation whose solution is

$$z(t) = z(0)\,\mathtt{exp}\left(-\int_0^t \alpha(\tau)d\tau\right). \qquad (A.11)$$

In order to study the evolution of $(h, \dot{h})$, we can consider two different cases, depending on the sign of the initial vertical velocity.

Case 1: $\dot{h}(0) < 0$. Let us show that $\dot{h}(t) < 0$, $\forall t$.
We make a proof by contradiction and assume that there exists t^* such that $\dot{h}(t^*) = 0$ and $\ddot{h}(t^*) \geq 0$. Then, according to (A.6), $\ddot{h}(t^*) < 0$. A clear contradiction.

Case 2: $\dot{h}(0) \geq 0$. If $\dot{h}(t)$ were always positive, or equal to zero, then, according to (A.10), $z(t)$ would be non-decreasing. This contradicts relation (A.11) which implies that $z(t)$ is strictly decreasing. Therefore there exists a time instant T such that $\dot{h}(T) < 0$, and we are brought back to Case 1 with T taken as the new origin of time.

By considering these two cases, we have shown that $\dot{h}(t)$ is strictly negative after a finite time. Let us now show that $h(t)$ and $\dot{h}(t)$ converge to zero. Since $h(t)$ is positive and decreases after a finite time-instant, it converges to some limit h_m which is either positive or equal to zero. Recall that the boundedness of ξ has already been proven so that $\xi_M := sup_{t\in[0,+\infty)}|\xi(t)|$ is a positive finite number. Let us assume that h_m is positive, then $\alpha(t) > \dfrac{h_m}{\xi_M} = \alpha_m > 0$, $\forall t$. Relation (A.11) then implies

$$z(0)\,e^{-\alpha_m t} > z(t) \geq z(0)\,e^{-t}\,,$$

and thus the convergence of $z(t)$ to zero. This in turn implies the convergence of $h(t)$ to zero, since $|\dot{h}(t)|$ $(\leq |v(t)|)$ is bounded. From this contradiction, one deduces that $h_m = 0$ and thus that $h(t)$ converges to zero.

Finally, using the fact that $k\alpha(t)$ is bounded and that $k/h(t)$ tends to infinity, the application of Lemma 3 to the equation (A.6) establishes the convergence of $\dot{h}(t)$ to zero.

Proof of item 3: We first show that the ratio $\frac{|v|}{h}$ is bounded. To this aim let us consider the equation governing the evolution of this ratio, as deduced from (A.4),

$$\frac{d}{dt}\left(\frac{|v|}{h}\right) = -\frac{k}{h}\left(\left[1 + \frac{\dot{h}}{k}\right]\frac{|v|}{h} + \cos(\beta)\right), \qquad (A.12)$$

with β the angle between v and ξ, so that $\cos(\beta) = \frac{v^T\xi}{|v||\xi|}$. Using the fact that k/h tends to infinity and that $\dot{h}/k$ tends to zero, the boundedness of $|v|/h$ is simply obtained by applying Lemma 4 to this equation. From there, the convergence of v to zero just follows from the convergence, previously proven, of h to zero.

Proof of item 4: Since

$$\frac{d}{dt}\left(\frac{\xi}{|\xi|}\right) = \left(I - \frac{\xi\xi^\top}{|\xi|^2}\right)\frac{v}{|\xi|},$$

and since $\frac{|v|}{|\xi|}$ $(\leq \frac{|v|}{h})$ tends to zero, the time-derivative of $\frac{\xi}{|\xi|}$ tends to zero, and is thus bounded. Consider now the dynamics of the ratio between $\dot{\xi}(t)$ and $h(t)$

$$\frac{d}{dt}\left(\frac{\dot{\xi}}{h}\right) = -\frac{k}{h}\left(\left[1+\frac{\dot{h}}{k}\right]\frac{\dot{\xi}}{h}+\frac{\xi}{|\xi|}\right), \tag{A.13}$$

The application of Lemma 5 to this equation yields

$$\left(\frac{\dot{\xi}}{h}+\frac{\xi}{|\xi|}\right)(t) = o(t). \tag{A.14}$$

Pre-multiplying both members of the above equality by $h\,\xi^\top$, one obtains the equation

$$\frac{d}{dt}|\xi|^2 + \bar{\alpha}(t)|\xi|^2 = 0$$

with

$$\bar{\alpha}(t) := 2\alpha(t)\left(1-\frac{\xi(t)^\top}{|\xi(t)|}\,o(t)\right),$$

whose solution must satisfy

$$|\xi(t)|^2 = |\xi(0)|^2 \exp\left(-\int_0^t \bar{\alpha}(s)\,ds\right). \tag{A.15}$$

Since h and $\dot{h}$ converge to zero, one deduces from (A.7) that the integral of α tends to $+\infty$. Therefore, by application of Lemma 6, the integral of $\bar{\alpha}$ also tends to $+\infty$. The convergence of ξ to zero then follows from the previous equality.

Proof of item 5: The boundedness of the control u_L given by (9) simply follows from the previously proven boundedness of v/h.

A.III Proof of Theorem 2

Consider the system (2) subjected to the control input (14) and use the following storage function:

$$\mathcal{L}_o = \mathcal{L} + \sum_{i=1}^n \phi_i, \tag{A.16}$$

whose time derivative

$$\dot{\mathcal{L}}_o = -k\frac{|v|^2}{h} - k_D\sum_{i=1}^n \frac{\dot{d}_i^2}{d_i}, \tag{A.17}$$

implies that $\mathcal{L}_o$ is bounded and, therefore, that $|v|$, $|\xi|$ and $\sum_{i=1}^n \phi_i$ are bounded.

Proof of item 1:

By proceeding analogously to the proof of theorem 1 (A.II, Item 1), it is straightforward to verify that $T_s = \infty$ and $h(t) > 0$, $\forall t$.

Proof of item 2:

The system is well defined and $\mathcal{L}_0$ is decreasing. The zeroing of $\dot{\mathcal{L}}_o = 0$ implies that the velocity vector is identically equal to zero and that the equilibrium $(\xi, v) = (\xi^*, 0) \neq (0,0)$ is a solution of the implicit equation $\ddot{\xi}^* = 0$. Therefore

$$k\frac{\xi^*}{|\xi^*|} = k_R\sum_{i=1}^n \gamma_i(\xi^*)p_i(\xi^*). \tag{A.18}$$

To prove the instability of the set E_u we only need to show that the closed-loop linearised system at an equilibrium point $(\xi, v) = (\xi^*, 0) \in E_u$ is unstable. The equation of the closed-loop system is:

$$\ddot{\xi} = -k\left(\frac{\dot{\xi}}{h}+\frac{\xi}{|\xi|}\right) + k_D\sum_{i=1}^n D_i p_i + k_R\sum_{i=1}^n \gamma_i p_i. \tag{A.19}$$

Setting $\pi_{\xi^*} = \left(I_3 - \frac{\xi^*}{|\xi^*|}\frac{\xi^{*\top}}{|\xi^*|}\right)$, the corresponding linearised system is $\dot{\chi} = A\chi$, with $\chi = (\xi, v)$, and

$$A = \left(\begin{array}{c|c} 0_3 & I_3 \\ \hline -k\frac{\pi_{\xi^*}}{|\xi^*|} - \sum_{i=1}^n k_R\left(\frac{\pi_{p_i}\gamma_i}{d_i}+\frac{p_i p_i^\top}{d_i}\right) & -\frac{I_3}{h} - k_o\sum_{i=1}^n \frac{p_i p_i^\top}{d_i} \end{array}\right)$$

where p_i, γ_i and d_i are evaluated at ξ^*. In view of eq. (A.18) it follows that:

$$\left|\sum_{i=1}^n \gamma_i p_i\right| = \frac{k}{k_R}$$

By choosing k_R small enough (with respect to k) the sum in the left-hand side of this equality can be rendered very large. Now, using the fact that the obstacles are scattered in the environment, it is simple to prove that making this sum tend to infinity is possible only if all γ_i's but one, say γ_j, remain bounded, so that

$$\sum_{i=1}^n \gamma_i(\xi^*)p_i(\xi^*) \approx \gamma_j(\xi^*)p_j(\xi^*) \tag{A.20}$$

Without loss of generality the index j can be omitted from now on, and the above approximation taken as an equality. Define $p = p_j$, $\gamma = \gamma_j$, and $d = d_j$. We now examine the eigenvalues of the matrix A.

To prove the instability of the matrix A, i.e. the positivity of at least one of its eigenvalues, it suffices to consider the first submatrix of the second block row

$$B = -k\frac{\pi_{\xi^*}}{|\xi^*|} - k_R\left(\frac{\pi_{p(\xi^*)}\gamma(\xi^*)}{d(\xi^*)}+\frac{p(\xi^*)p(\xi^*)^\top}{d(\xi^*)}\right), \tag{A.21}$$

and show that this matrix is itself unstable.
Note that $\frac{\xi^*}{|\xi^*|} = \pm p(\xi^*)$. Using the fact that there exists a rotation matrix Q such that $p(\xi^*) = Qe_3$, eq. (A.21) can be written as

$$B = Q\left(-\left(\frac{k}{|\xi^*|}+\frac{k_R\gamma(\xi^*)}{d(\xi^*)}\right)\pi_{e_3} - \frac{k_R}{d(\xi^*)}e_3e_3^\top\right)Q^\top.$$

At the equilibrium it follows from (A.18) and (A.20) that $\gamma = -\frac{k}{k_R}$. Therefore, one gets

$$B = Q\left(-k\left(\frac{1}{|\xi^*|}-\frac{1}{d(\xi^*)}\right)\pi_{e_3} - \frac{k_R}{d(\xi^*)}e_3e_3^\top\right)Q^\top, \tag{A.22}$$

whose eigenvalues are

$$\left\{-k\left(\frac{1}{|\xi^*|}-\frac{1}{d}\right), -k\left(\frac{1}{|\xi^*|}-\frac{1}{d}\right), -\frac{k_R}{d}\right\}. \tag{A.23}$$

Since $d(\xi^*) < |\xi^*|$, the first two eigenvalues are positive and hence the matrix B (and therefore A) is unstable.